Mechanistic approaches for chemically modifying the coordination sphere of copper–amyloid-β complexes

Jiyeon Han[a], Hyuck Jin Lee[a,b], Kyu Yeon Kim[c], Geewoo Nam[d], Junghyun Chae[c], and Mi Hee Lim[a,1]

[a]Department of Chemistry, Korea Advanced Institute of Science and Technology, 34141 Daejeon, Republic of Korea; [b]Department of Chemistry Education, Kongju National University, 32588 Gongju, Republic of Korea; [c]Department of Chemistry, Sungshin Women's University, 02844 Seoul, Republic of Korea; and [d]Department of Chemistry, Ulsan National Institute of Science and Technology, 44919 Ulsan, Republic of Korea

Edited by Marcetta Y. Darensbourg, Texas A&M University, College Station, TX, and approved January 27, 2020 (received for review September 29, 2019)

Neurotoxic implications of the interactions between Cu(I/II) and amyloid-β (Aβ) indicate a connection between amyloid cascade hypothesis and metal ion hypothesis with respect to the neurodegeneration associated with Alzheimer's disease (AD). Herein, we report a mechanistic strategy for modifying the first coordination sphere of Cu(II) bound to Aβ utilizing a rationally designed peptide modifier, L1. Upon reacting with L1, a metal-binding histidine (His) residue, His14, in Cu(II)–Aβ was modified through either covalent adduct formation, oxidation, or both. Consequently, the reactivity of L1 with Cu(II)–Aβ was able to disrupt binding of Cu(II) to Aβ and result in chemically modified Aβ with altered aggregation and toxicity profiles. Our molecular-level mechanistic studies revealed that such L1-mediated modifications toward Cu(II)–Aβ could stem from the molecule's ability to 1) interact with Cu(II)–Aβ and 2) foster copper–O_2 chemistry. Collectively, our work demonstrates the development of an effective approach to modify Cu(II)–Aβ at a metal-binding amino acid residue and consequently alter Aβ's coordination to copper, aggregation, and toxicity, supplemented with an in-depth mechanistic perspective regarding such reactivity.

copper | amyloid-β | small molecule | copper–O_2 chemistry | residue-specific modifications

Transition metal ions are critical components in the nervous systems, playing various structural and catalytic roles (1–3). In particular, copper is an indispensable element for energy metabolism, antioxidant defense, and the synthesis of neurotransmitters (4–7). Thus, the uptake and efflux of intracellular copper are tightly regulated in the brain (4, 6). Upon copper ion dyshomeostasis, vital copper-mediated functions become compromised with neurotoxicity observed in neurodegenerative disorders such as Alzheimer's disease (AD) (4–9).

In the AD-afflicted brain, copper can be detected at concentrations as high as 400 μM in senile plaques, mainly composed of amyloid-β (Aβ) aggregates (4). The complexation between Cu(II) and Aβ and its neurotoxic implications have been previously reported (4, 8–12). The first coordination sphere of Cu(II) bound to Aβ typically consists of three nitrogen (N) donor atoms and one oxygen (O) donor atom, as depicted in Fig. 1*A* (11, 13). The N donor atoms consist of a combination of two histidine (His) residues (i.e., His6 and His13 or His14), an amide backbone, and the primary amine at the amino terminus (N terminus), while a carbonyl backbone between Asp1 and Ala2 serves as the O donor atom under physiological conditions (13, 14). The dissociation constant (K_d) of Cu(II) for Aβ is approximately 10^{-10} M (4, 11, 12, 15). Cu(II) binding to Aβ can accelerate Aβ aggregation and stabilize toxic structured Aβ oligomers (4, 16–18). In addition, redox-active Cu(I/II)–Aβ complexes can overproduce reactive oxygen species (ROS) via Fenton-like reactions, contributing to oxidative stress (4, 15, 19, 20).

In an effort to regulate the reactivities of Cu(II)–Aβ complexes such as their aggregation and ROS generation, several metal chelators have been utilized to extract copper from Cu(II)–Aβ (21–26). Furthermore, rationally designed small molecules were reported to form a ternary complex with Cu(II)–Aβ and consequently change its properties (27–29). Upon reacting with such small molecules, Cu(II)–Aβ was indiscriminately oxidized (29), suggesting the potential significance of copper–O_2 chemistry to modify Aβ (15, 19, 20). In this study, we hypothesize that specifically transforming the coordination sphere of Cu(II)–Aβ can be an effective strategy for disrupting Cu(II) binding to Aβ and chemically modifying Aβ to alter its aggregation and toxicity profiles. Herein, a mechanistic strategy is presented for specifically modifying His14, an amino acid residue involved in Cu(II)–Aβ coordination, through either covalent bond formation, oxidation, or both (Fig. 1*A*).

Results

Design and Preparation of a Small Molecule as a Peptide Modifier toward Cu(II)–Aβ. Three main criteria were considered in designing our peptide modifier, **L1** (Fig. 1*B*): 1) the accommodation of the coordination geometries for both Cu(I) and Cu(II) centers with respect to the formation of transient ternary complexes with Cu(I/II)–Aβ; 2) the redox potential of the designed molecule; and 3) the promotion of copper–O_2 chemistry for Cu(I/II)–Aβ. First, to tailor the bidentate coordination to the copper center of Cu(I/II)–Aβ complexes, the sulfur (S) and N donor atoms in thiophen-2-ylmethanamine and the *N*,*N*-dimethylaniline (**DMA**) moiety, reported to be important for interacting with Cu(I/II) and Aβ, respectively (29, 30), were incorporated to produce **L1**. Under the assumption that redox chemistry of Cu(I/II)–Aβ at the

Significance

Metal ions in the brain exhibit both functional (e.g., signal transduction, oxidative metabolism, and antioxidant defense) and pathological qualities (e.g., oxidative damage). Impaired metal ion homeostasis is linked to the decrease in enzymatic activities, the elevation of protein aggregation, and oxidative stress, leading to neurodegeneration. Particularly, copper coordinates to amyloid-β (Aβ) peptides, a pathological factor of Alzheimer's disease, facilitating Aβ aggregation and inducing oxidative stress. Our work presents a mechanistic strategy to modify the coordination sphere of Cu(II) bound to Aβ using a chemical reagent by promoting copper–O_2 chemistry, which can inhibit Cu(II) binding to Aβ and alter Aβ's aggregation and toxicity. Our multidisciplinary studies demonstrate a direction for modulating copper-interacting amyloidogenic proteins.

Author contributions: J.H. and M.H.L. designed research; J.H. and H.J.L. performed research; K.Y.K. and J.C. contributed new reagents/analytic tools; J.H., H.J.L., G.N., and M.H.L. analyzed data; and J.H., G.N., and M.H.L. wrote the paper.

The authors declare no competing interest.

This article is a PNAS Direct Submission.

[1]To whom correspondence may be addressed. Email: miheelim@kaist.ac.kr.

This article contains supporting information online at https://www.pnas.org/lookup/suppl/doi:10.1073/pnas.1916944117/-/DCSupplemental.

First published February 26, 2020.

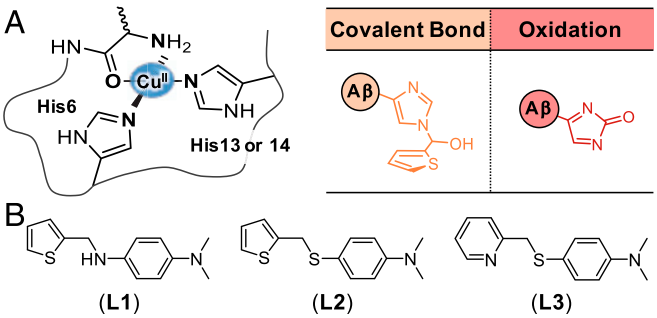

Fig. 1. Modifications at the Cu(II) coordination site and small molecules studied in this work. (*A*) Chemical modifications obtained from the reaction of Cu(II)–Aβ with **L1**. (*B*) Chemical structures of **L1** [N^1,N^1-dimethyl-N^4-(thiophen-2-ylmethyl)benzene-1,4-diamine], **L2** [*N*,*N*-dimethyl-4-((thiophen-2-ylmethyl)thio)aniline], and **L3** [*N*,*N*-dimethyl-4-((pyridin-2-ylmethyl)thio)aniline].

copper center accounts for a major facet of a compound's ability to modify Aβ, the chemical structure of **L1** manifests S and N donor atoms anticipated to accommodate the coordination geometries of both Cu(I) and Cu(II) bound to Aβ based on the hard soft acid base (HSAB) principle. The redox potential of **L1** was also considered with respect to the redox cycling between Cu(I)–Aβ and Cu(II)–Aβ. The redox property of the *N*,*N*-dimethyl-*p*-phenylenediamine (**DMPD**) moiety in **L1** {$E_{1/2}$: 0.11 V vs. Ag/Ag(I) in H_2O (31, 32)} could be critical in the molecule's capacity as a reducing agent for Cu(II)–Aβ {E^0: approximately 0.083 V vs. Ag/Ag(I) in H_2O (33)}. Lastly, the thiophene moiety acts as a weak σ-bonding ligand for copper (34), which suggests the potential for O_2 binding at the metal center in Cu(I/II)–Aβ to promote copper–O_2 chemistry leading to modifications of Aβ.

Based on the structure and properties of **L1** as well as previous reports of copper–O_2 chemistry (35–37), chemical transformation and reactivity of the compound toward Cu(II)–Aβ may be expected. For instance, *N*-dealkylation of **L1** can be driven by Cu(I/II)–O_2 chemistry to yield thiophen-2-carboxaldehyde (**TCA**) and **DMPD** (Scheme 1*A*) (38). Both **TCA** and **DMPD** may then undergo the conjugation with Aβ through multiple nucleophilic amino acid residues (31, 39). Moreover, oxidation of **L1** to its radical cation ($L1^{+\bullet}$) can drive the reduction of Cu(II)–Aβ to Cu(I)–Aβ. The resultant Cu(I)–Aβ could then react with O_2 to generate copper–O_2 intermediates and subsequently modify Aβ (Scheme 1*B*).

To better understand the structure-to-function relationship of **L1**, two additional compounds, **L2** and **L3**, were constructed by replacing the C–N bond of **L1** with a C–S bond (Fig. 1*B*). The **DMA** moiety, thought to be important for interacting with Aβ (29, 30), was maintained. The metal-interacting portions were also retained by incorporating a thiophen-2-ylmethanethioether group and a pyridin-2-ylmethanethioether group for **L2** and **L3**, respectively. According to the HSAB theory, **L2** can exhibit difficulty in accommodating the coordination geometries of both Cu(I) and Cu(II); **L3** can be bound to both Cu(I) and Cu(II), similar to **L1** (34). Both **L2** and **L3** are expected to be less oxidizable in comparison to **L1** based on their structural portion, *N*,*N*-dimethyl-4-(methylsulfanyl)aniline (32). Overall, structural distinctions between **L1** and **L2** or **L3** could allow us to investigate the significance of a molecule's ability to directly bind to Cu(II)–Aβ and foster redox chemistry at the copper center to drive copper–O_2 chemistry and, ultimately, modify Aβ.

As depicted in *SI Appendix*, Scheme S1, **L1**, **L2**, and **L3** were prepared through reductive amination or substitution reactions. Detailed information for the synthesis and characterization of the compounds is provided in the *SI Appendix*, Scheme S1 and Figs. S1–S3. **L1**, **L2**, and **L3** are predicted to cross the blood–brain barrier (BBB) with logBB values (logarithm of the ratio of the concentration of the compound in the brain to concentration in the blood) of 0.345, 0.702, and 0.338 and adhering to the Lipinski rule, as shown in *SI Appendix*, Table S1 (40, 41). In addition to the theoretical logBB values, the experimental permeability values ($-\log P_e$) of the compounds were obtained by the in vitro parallel artificial membrane-permeability assay adapted for the BBB (PAMPA–BBB). The values of $-\log P_e$ of **L1**, **L2**, and **L3** were 4.31 (± 0.13), 4.61 (± 0.22), and 4.35 (± 0.07), respectively, indicating the potential of the molecules to penetrate the BBB (40, 41).

Modifications of the Coordination Sphere of Cu(II)–Aβ. Cu(II)–Aβ complexes upon treatment with **L1**, **L2**, and **L3** were analyzed by electrospray ionization–mass spectrometry (ESI–MS) and tandem MS (ESI–MS^2). The sample of $Aβ_{40}$ incubated with Cu(II)

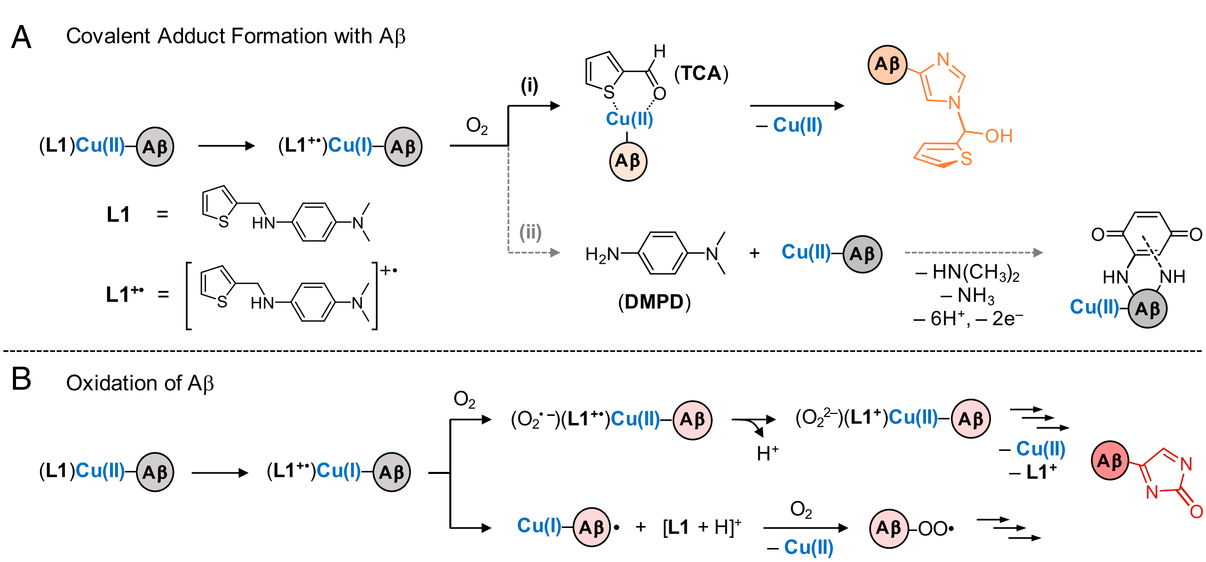

Scheme 1. Potential mechanisms for His14-specific modifications obtained upon the reaction of Cu(II)–Aβ with **L1**: (*A*) covalent adduct formation with Aβ and (*B*) oxidation of Aβ.

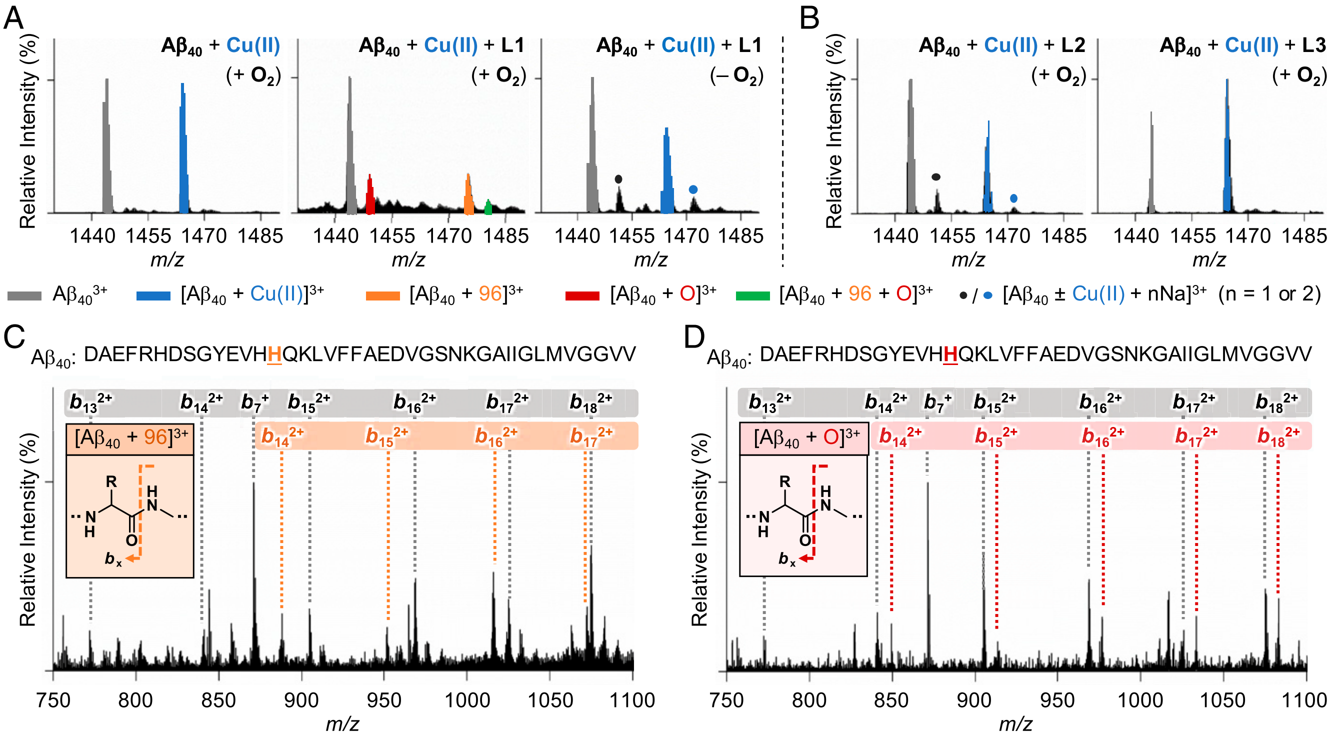

Fig. 2. Analysis of Cu(II)-treated $A\beta_{40}$ upon incubation with **L1** by ESI–MS and ESI–MS^2. (*A*) ESI–MS spectra of the +3-charged Cu(II)-added $A\beta_{40}$ monomer incubated with **L1** in the absence and presence of O_2. (*B*) ESI–MS spectra of the +3-charged Cu(II)-added $A\beta_{40}$ monomer treated with **L2** and **L3** under aerobic conditions. The peaks of the covalent adduct between $A\beta_{40}$ and 2-methylthiophene (1,475 *m/z*) and the singly oxidized $A\beta_{40}$ (1,449 *m/z*) are highlighted in orange and red, respectively. The singly oxidized covalent adduct (1,480 *m/z*) is presented as a green peak. Na^+ adducts of $A\beta_{40}$ with or without Cu(II) are shown with blue and black dots. (*C* and *D*) ESI–MS^2 spectra of the covalent adduct (1,475 *m/z*) and the singly oxidized peptide (1,449 *m/z*). The gray, orange, and red boxes indicate b_x fragments corresponding to Aβ, Aβ bound to 2-methylthiophene, and singly oxidized Aβ, respectively. Conditions were as follows: $[A\beta_{40}]$, 100 μM; $[CuCl_2]$, 100 μM; [compound], 500 μM; incubation for 1 h; 20 mM ammonium acetate, pH 7.2; 37 °C; no agitation. The samples were diluted with H_2O by 10-fold prior to injection to the mass spectrometer.

indicated a peak corresponding to Cu(II)-bound $A\beta_{40}$ at 1,464 *m/z* (Fig. 2*A*). When **L1** was introduced to Cu(II)–$A\beta_{40}$, new peaks indicating modifications of Aβ were detected at 1,449, 1,475, and 1,480 *m/z* (vide infra for mechanistic details): corresponding to oxidation, covalent adduct formation, and dual-modification (both oxidation and covalent adduct formation), respectively. **L2** and **L3** did not noticeably affect Cu(II) binding to $A\beta_{40}$, as presented in Fig. 2*B*. In the absence of Cu(II), such mass shifts from $A\beta_{40}$ were not induced by the compounds (*SI Appendix*, Fig. S4).

Covalent adduct formation. Upon analyzing the Cu(II)–$A\beta_{40}$ sample treated with **L1**, a new peak was detected at 1,475 *m/z*, assigned as $[A\beta_{40} + 96]^{3+}$ (Fig. 2*A*, orange peak). To identify the modified amino acid residue, ESI–MS^2 was performed for the selected ion at 1,475 *m/z*. Note that the collision-induced dissociation (CID) of the target ion results in the detection of *b* fragments, which could be analyzed for residue-specific peptide modifications (32, 42). Upon applying the CID to the peak at 1,475 *m/z*, a mass shift of 96 Da was observed from b_{14}, suggesting that His14 was transformed by **L1** (Fig. 2*C*).

The peak at 1,475 *m/z* is suspected to be a product of the reaction between His14 and **TCA**, an *N*-dealkylation product of **L1** mediated by copper–O_2 chemistry, as shown in Scheme 1*A*, (i) (35, 38). The interaction between **TCA** and Cu(II)–Aβ may form a transient ternary **TCA**–Cu(II)–Aβ complex, as shown in Scheme 1*A*, (i), where the aldehyde group in **TCA** could be subject to a nucleophilic attack by a proximal amino acid residue in Aβ (e.g., His14) (43). Thus, an increase in 96 Da from $A\beta_{40}$ could be assigned to Aβ covalently bound to the 2-methylthiophene moiety. Note that 2-methylthiophene could be produced through the dehydration of thiophene-2-ylmethanol. Such dehydration of molecules is frequently observed in mass spectrometric studies (44). To further confirm the role of **L1**'s transformation to **TCA** in covalently modifying Cu(II)–Aβ, the Cu(II)–Aβ sample directly treated with **TCA** was analyzed by ESI–MS. A peak corresponding to $[A\beta_{40} + 96]^{3+}$ was also detected at 1,475 *m/z* in the sample incubated with **TCA** (*SI Appendix*, Fig. S5). ESI–MS^2 studies showed that the His14 residue in $A\beta_{40}$ was modified by **TCA** in the presence of Cu(II), indicating that copper–O_2 chemistry driving *N*-dealkylation of **L1** is essential for generating the covalent adduct with $A\beta_{40}$.

Oxidation. Upon incubation of Cu(II)–$A\beta_{40}$ with **L1**, a peak denoting a mass shift of 16 Da from monomeric $A\beta_{40}$ was monitored at 1,449 *m/z*, as depicted in Fig. 2*A* (red peak). ESI–MS^2 revealed that this mass shift took place starting from b_{14}, indicating the modification of His14 by treatment of **L1** in the presence of Cu(II) (Fig. 2*D*). Such His14 modification affects Cu(II) binding to Aβ, as evidenced by the decrease in the peak intensity of Cu(II)–Aβ, as shown in Fig. 2*A*.

The peak at 1,449 *m/z* could denote **L1**-mediated oxidation of monomeric $A\beta_{40}$. Aβ oxidation may occur through a process involving the reduction of Cu(II)–Aβ to Cu(I)–Aβ coupled with the oxidation of **L1** to its cationic radical, $\mathbf{L1}^{+\bullet}$, as described in Scheme 1*B* {E^0 [for Cu(II)–Aβ]: approximately 0.083 V (33); $E_{1/2}$ (for **L1**): 0.098 V (*SI Appendix*, Fig. S6; vide infra) vs. Ag/Ag(I) in H_2O, respectively, at a similar scan rate}. Cu(I)–Aβ can then react with O_2 to form a transient intermediate such as $Cu(II)(A\beta_{40})(O_2^{\bullet-})(\mathbf{L1}^{+\bullet})$ and $Cu(II)(A\beta_{40})(O_2^{2-})(\mathbf{L1}^{+})$ under aerobic conditions (Scheme 1*B*, top reaction) (10, 45, 46), finally resulting in the oxidation of Aβ (e.g., His oxidation) (47). In parallel, $L1^{+\bullet}$ could abstract a hydrogen atom from Aβ to form a carbon-centered peptide radical that may further interact with O_2 to produce a peroxyl radical form of Aβ followed by peptide oxidation (Scheme 1*B*, bottom reaction) (48). To determine whether the transformation of **L1** to **TCA** and **DMPD** is a prerequisite process for the oxidation of Aβ (Scheme 1*A*), the samples containing Cu(II) and $Aβ_{40}$ with **TCA** or **DMPD** were prepared separately and analyzed under the same conditions used to study **L1**. Oxidation of $Aβ_{40}$ was not observed in the **TCA**-containing samples, while **DMPD** oxidized Lys16, not His14, as shown in *SI Appendix*, Figs. S5 and S7, the latter of which is in agreement with previously reported results (31). These data suggest that such peptide oxidation at His14 occurs through the oxidation of **L1** in the presence of Cu(II)–Aβ over the compound's *N*-dealkylation to **TCA** and **DMPD**.

To further confirm that the His14-specific oxidation of Aβ is mediated by **L1**, the peptide oxidation by ROS, broadly present in biological systems, was investigated. More specifically, $Aβ_{40}$ incubated with hydrogen peroxide (H_2O_2) was analyzed by ESI–MS, the dot blot assay, and transmission electron microscopy (TEM) (*SI Appendix*, Figs. S8 and S9). Upon treatment of H_2O_2 to metal-free $Aβ_{40}$, the oxidation of Met35 was solely observed (*SI Appendix*, Fig. S8), as reported previously (49). In the case of Cu(II)-treated $Aβ_{40}$ with H_2O_2, all ESI–MS peaks from $Aβ_{40}$ completely disappeared under our experimental conditions (*SI Appendix*, Fig. S9*A*). To verify the modified regions in $Aβ_{40}$, the dot blot assay employing an anti-Aβ antibody, 6E10 (for N terminus) (27), and an anti-$Aβ_{40}$ antibody (for carboxyl terminus [C terminus]) (50) was carried out (*SI Appendix*, Fig. S9 *B* and *C*). Upon incubation of Cu(II)–$Aβ_{40}$ with H_2O_2 for 1 and 24 h, the signal intensity of 6E10 was noticeably decreased, indicating that H_2O_2 modified the $Aβ_{16}$ region of Cu(II)–$Aβ_{40}$, whereas the dot blot using the anti-$Aβ_{40}$ antibody showed a similar signal intensity to that of the H_2O_2-free control samples, suggesting that the C terminus was not altered. In order to clarify the effects of H_2O_2 on the fibrillization of Cu(II)–$Aβ_{40}$, the dot blot assay using an anti-fibril antibody (OC) (51) and TEM were performed (*SI Appendix*, Fig. S9 *B* and *C*). Upon incubation with H_2O_2 for 1 h, Cu(II)–$Aβ_{40}$ exhibited the signal of OC at a level comparable to that of the H_2O_2-free control sample. At 24 h incubation of H_2O_2 with Cu(II)–$Aβ_{40}$, the signal intensity of OC was significantly reduced, possibly due to the altered aggregation of Cu(II)–$Aβ_{40}$. The presence of H_2O_2 varied the overall size and shape of the resultant $Aβ_{40}$ aggregates, as visualized by TEM. The morphologies of H_2O_2- and **L1**-treated Aβ aggregates were notably different (for H_2O_2-treated aggregates, see *SI Appendix*, Fig. S9 *B* and *C*; vide infra for **L1**-incubated Aβ aggregates). These observations support that the His14-specific oxidation toward Cu(II)–Aβ mediated by **L1** is distinct from the peptide oxidation by general oxidants.

Dual-modification. The peak detected at 1,480 *m/z* was assigned as $[Aβ_{40} + 96 + O]^{3+}$ (green peak in Fig. 2*A*). This peak implicates the dual-modification of $Aβ_{40}$ (both covalent bond formation and oxidation). To verify which amino acid residue was chemically modified by **L1**, $ESI–MS^2$ was performed for the singly oxidized covalent adduct at 1,480 *m/z*. As illustrated in *SI Appendix*, Fig. S10, covalent adduct formation, oxidation, and both were detected from b_{14}.

Taken together, **L1** was able to chemically modify the metal-binding residue, His14, in Cu(II)–$Aβ_{40}$ through either covalent bond formation, oxidation, or both. Such modifications could disrupt the complexation between Cu(II) and Aβ and change the secondary structure of the resultant Aβ, which was supported by the results obtained by inductively coupled plasma–MS (ICP–MS) and circular dichroism (CD) spectroscopy, respectively. Upon incubation of **L1** with Cu(II)–$Aβ_{40}$, the concentration of free copper in the supernatant was noticeably increased in comparison to that of the **L1**-free sample, detected by ICP–MS (*SI Appendix*, Fig. S11). This observation suggests that **L1**-mediated peptide modifications can dissociate copper from $Aβ_{40}$. Moreover, a slight change in the secondary structure of $Aβ_{40}$ was monitored by CD spectroscopy, when Cu(II)-added $Aβ_{40}$ was treated with **L1** for 24 h (α-helix, 6.1 to 0%; β-strand, 26 to 34%) (*SI Appendix*, Fig. S12).

Cu(II)–Aβ-Mediated Transformations of L1. To determine the molecular mechanisms regarding **L1**-mediated modifications at the coordination sphere of Cu(II)–Aβ, the transformation of **L1**, **L2**, and **L3** was investigated in the presence of Cu(II) and Aβ through ultraviolet–visible spectroscopy (UV–vis), ESI–MS, and cyclic voltammetry (Fig. 3 and *SI Appendix*, Figs. S13–S16).

Cleavage. *N*-dealkylation of **L1** to generate **TCA** and **DMPD** in the presence of Cu(II) with or without $Aβ_{40}$ was monitored by UV–vis

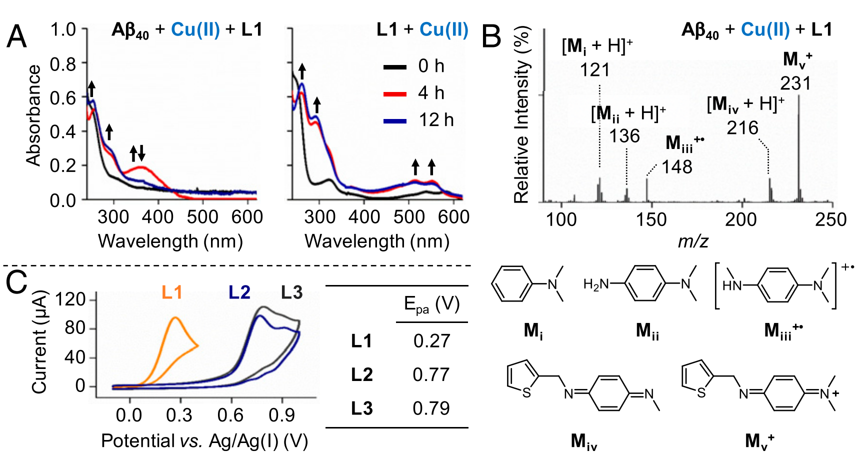

Fig. 3. Transformations and anodic peak potentials (E_{pa}) of **L1**, **L2**, and **L3**. (*A*) Optical changes of **L1** upon addition of Cu(II) with and without $Aβ_{40}$ under aerobic conditions. The new appearance of the peaks is indicated with black arrows. Conditions were as follows: [$Aβ_{40}$], 25 μM; [$CuCl_2$], 25 μM; [compound], 50 μM; room temperature; incubation for 1 h (black), 4 h (red), and 12 h (blue). (*B*) Structural variations of **L1** in the presence of Cu(II)-treated $Aβ_{40}$, monitored by ESI–MS. Conditions were as follows: [$Aβ_{40}$], 100 μM; [$CuCl_2$], 100 μM; [**L1**], 500 μM; incubation for 1 h; 20 mM ammonium acetate, pH 7.2; 37 °C; no agitation. The sample was diluted with H_2O by 10-fold prior to injection to the mass spectrometer. (*C*) Cyclic voltammograms of **L1**, **L2**, and **L3** in DMSO at the scan rate of 250 mV/s. The E_{pa} values of the compounds at various scan rates are summarized in *SI Appendix*, Table S2. Conditions were as follows: [compound], 1 mM; 0.1 M *tetra-N*-butylammonium perchlorate; room temperature; three electrodes composed of the glassy carbon working electrode, platinum counter electrode, and Ag/Ag(I) reference electrode.

and ESI–MS. As illustrated in Fig. 3*A*, when **L1** was incubated with $CuCl_2$ and $A\beta_{40}$, an increase in absorbance at approximately 375 nm followed by the disappearance of the same peak after 12 h was observed. This absorption band at approximately 375 nm may correspond to the charge transfer between **L1** and Cu(II)–$A\beta_{40}$ or the quinone-imine moiety of $\mathbf{L1^+}$ (vide infra) (52). Additionally, the peaks at approximately 260 and 300 nm were slightly enhanced, indicating the presence of a mixture of **TCA** and **DMPD**. **DMPD** was also detected by ESI–MS ($\mathbf{M_{ii}}$ in Fig. 3*B*) upon treatment of **L1** with Cu(II)–$A\beta_{40}$. Under $A\beta_{40}$-free conditions, the optical bands of Cu(II)-treated **L1** at 260 and 300 nm were noticeably increased, as depicted in Fig. 3*A*, suggesting the production of both **TCA** and **DMPD**. Fragmentation of **L1** in the presence of Cu(II) without Aβ was also confirmed by ESI–MS (*SI Appendix*, Fig. S13*A*).

Unlike **L1**, **L2** did not undergo notable transformation in the presence of Cu(II) or Cu(II)–Aβ under our experimental conditions, as shown in *SI Appendix*, Figs. S13*B* and S14*A*. Interaction between the compound and Cu(II) manifested a charge transfer band in the range from approximately 300 to 500 nm. In the case of **L3**, no significant optical changes were observed upon incubation with Cu(II) or Cu(II)–Aβ (*SI Appendix*, Fig. S14*B*), but a peak at 261 *m/z* was detected by ESI–MS from the sample containing Cu(II)–Aβ and the compound, implicating the oxidation of its thioether moiety (*SI Appendix*, Fig. S13*B*). *N*-dealkylation of **L2** and **L3** was not observed, indicating that these two compounds do not couple with the copper–O_2 chemistry discussed above for **L1**.

Oxidation. When **L1** was incubated with Cu(II)–$A\beta_{40}$, $\mathbf{L1^{+\bullet}}$ was not detected by either ESI–MS or UV–vis, as indicated in Fig. 3 *A* and *B*. Instead, the two-electron oxidized form, $\mathbf{L1^+}$ ($\mathbf{M_v}^+$; Fig. 3*B*), was monitored in the low molecular-weight region of the ESI–MS spectrum from the sample containing **L1** and Cu(II)–$A\beta_{40}$. In the presence of Cu(II) without $A\beta_{40}$, the peak at 232 *m/z* corresponding to $\mathbf{L1^{+\bullet}}$ was detected by ESI–MS (*SI Appendix*, Fig. S13*A*). Moreover, as presented in Fig. 3*A*, the absorbance peaks at approximately 500 and 550 nm were displayed upon incubation of **L1** and Cu(II), indicative of the one-electron oxidation of the compound (31, 32). These double peaks may also represent the one-electron oxidation of **DMPD** (i.e., $\mathbf{DMPD^{+\bullet}}$) (31), an *N*-dealkylation product of **L1** (Scheme 1*A*). Note that such optical changes were not notably observed in the absence of Cu(II) under our experimental conditions (*SI Appendix*, Fig. S15). In the case of **L2** and **L3**, neither one- nor two-electron oxidation was monitored in the presence of Cu(II) with and without Aβ, as depicted in *SI Appendix*, Figs. S13*B* and S14, suggesting that these two compounds may not be able to reduce Cu(II)–Aβ to Cu(I)–Aβ, a prerequisite for inducing the oxidation of Aβ.

In addition to the spectroscopic and spectrometric studies, the redox potentials of **L1**, **L2**, and **L3** were measured at various scan rates in dimethyl sulfoxide (DMSO) and H_2O, as summarized in Fig. 3*C* and *SI Appendix*, Figs. S6 and S16. Due to the irreversible nature of the electrochemical waves in DMSO (*SI Appendix*, Fig. S16 and Table S2), the $E_{1/2}$ values could not be obtained. The anodic peak potential (E_{pa}) of **L1** was 0.27 V at 250 mV/s vs. Ag/Ag(I), which is significantly lower than those of **L2** (0.77 V) and **L3** (0.79 V) at the same scan rate. It can be inferred from the difference in the E_{pa} values of the abovementioned molecules that the **DMPD** moiety may be responsible for stabilizing $\mathbf{L1^{+\bullet}}$, as reported previously (29, 32). Under aqueous conditions, the $E_{1/2}$ value of **L1** was determined as 0.10 V, which is lower than that of **L3** (0.51 V) at 250 mV/s (*SI Appendix*, Fig. S6 and Table S3). Note that the cyclic voltammogram of **L2** in H_2O could not be obtained due to its limited solubility. The comparable redox potentials of Cu(II)–$A\beta_{42}$ and **L1** [approximately 0.083 V (33) and 0.098 V vs. Ag/Ag(I) in H_2O with a similar scan rate] suggest that Cu(II)–Aβ could be reduced to Cu(I)–Aβ upon oxidation of **L1**. Together, *N*-dealkylation of **L1** coupled with copper–O_2 chemistry could yield **TCA** and **DMPD**, the former of which may be required for the covalent adduct formation with Aβ in the presence of Cu(II). Furthermore, the oxidation of **L1** conjugated with the reduction of Cu(II)–Aβ to Cu(I)–Aβ could direct the oxidation of His14.

Specificity of L1-Induced Dual-Modification against Cu(II)–Aβ. To confirm that our proposed mechanism for **L1**-induced modifications toward Cu(II)–Aβ is driven by the direct interaction between **L1** and Cu(II)–Aβ and copper–O_2 chemistry (Scheme 1), additional ESI–MS studies employing multiple metal ions and proteins were performed. In the absence of O_2, Cu(I) and Cu(II) could not induce the modification of Aβ even with the treatment of **L1**, as shown in Fig. 2*A* and *SI Appendix*, Fig. S17*A*. The presence of Cu(I) without **L1**, under aerobic conditions, did not result in any notable modifications of Aβ. In the presence of O_2, **L1** induced the covalent adduct formation and the oxidation at His14 in the sample of Cu(I)–Aβ, as observed upon treatment of Cu(II)–Aβ with **L1** (*SI Appendix*, Fig. S17 *B*–*D*). Based on the lack of noticeable reactivity against Aβ in the absence of either Cu(I/II) or O_2, it can be inferred that **L1**'s capacity for altering His14 in Aβ requires the direct interaction with Cu(II)–Aβ to foster the underlying copper–O_2 chemistry presented in Scheme 1.

The pertinent role of the redox chemistry presented by Cu(I/II) indicates the potential of other redox-active metal ions for driving **L1**-mediated Aβ modifications. This notion was directly investigated with three redox-active metal ions [i.e., Fe(II), Fe(III), Co(II)] and a redox-inactive metal ion [i.e., Zn(II)]. Interestingly, the presence of Fe(II), Fe(III), Co(II), and Zn(II) did not prompt the His14-specific modifications of Aβ that were induced by **L1** in the presence of Cu(I/II). Upon introduction of Fe(II) to $A\beta_{40}$, the Fe(II)–$2A\beta_{40}^{5+}$ complex was detected; however, no modification of Aβ was observed with the treatment of **L1** (*SI Appendix*, Fig. S18 *A*, *Top*). Upon incubation of Fe(III)-added $A\beta_{40}$ with **L1**, Fe(III) binding to $A\beta_{40}$ was not found, and no discernible new peaks were observed relative to the control (*SI Appendix*, Fig. S18 *A*, *Bottom*). The analysis of the sample containing Co(II)-treated $A\beta_{40}$ with **L1** led to the detection of the Co(II)–$A\beta_{40}^{3+}$ complex, along with $A\beta_{12}^+$ at 1,424 *m/z* (*SI Appendix*, Fig. S18*B*), previously reported to indicate the hydrolytic cleavage of $A\beta_{40}$ (53). Lastly, when redox-inactive Zn(II) was incubated with $A\beta_{40}$ in the presence of **L1**, Zn(II) was able to bind to $2A\beta_{40}^{5+}$, but **L1** did not trigger any modifications of Aβ (*SI Appendix*, Fig. S18*C*). Based on our spectrometric analyses of the Aβ samples incubated with Cu(I/II), Fe(II/III), Co(II), and Zn(II), the dual-modification of Aβ by **L1** at His14 appears to exhibit a degree of specificity toward Cu(II)–Aβ.

To further confirm that such dual-modification by **L1** is specific for Cu(II)–Aβ, the interactions of **L1** with α-synuclein (α-Syn) and human islet amyloid polypeptide (hIAPP) (amyloidogenic) and ubiquitin (nonamyloidogenic) in the presence of Cu(II) were further analyzed by ESI–MS (*SI Appendix*, Fig. S19). The covalent adduct formation between **L1** and the three abovementioned proteins was not observed even with Cu(II). In the case of oxidation, a mass shift by 16 Da from α-Syn or Cu(II)-bound hIAPP was indicated in the samples of Cu(II)-added proteins and **L1**. Note that the oxidized residue could not be determined due to limitations on resolution. No oxidation of ubiquitin was shown following treatment of both Cu(II) and **L1**. Overall, these results suggest that the **L1**-induced dual-modification is specific toward Cu(II)–Aβ.

Modulation of Cu(II)–Aβ Aggregation. To identify whether **L1**-induced modifications at His14 affect the aggregation of Cu(II)–Aβ, the size distribution and morphology of the resultant Aβ species were verified by gel electrophoresis with Western blotting (gel/Western blot) and TEM, respectively. Note that the thioflavin-T assay could not be performed in this study due to the interference of the absorption of **L1** with the fluorescence window for analysis.

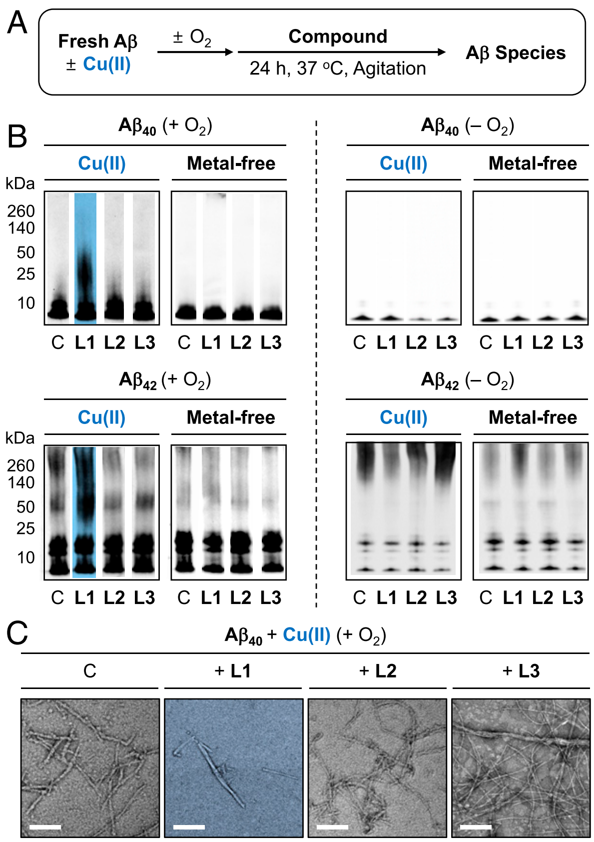

Fig. 4. Influence of **L1**, **L2**, and **L3** on the aggregation of Cu(II)-bound and metal-free Aβ. (*A*) Scheme of the inhibition experiments. (*B*) Analysis of the size distribution of the resultant $Aβ_{40}$ and $Aβ_{42}$ species in the presence (*Left*) and absence (*Right*) of O_2 by gel/Western blot using an anti-Aβ antibody (6E10). Lanes are as follows: C, Aβ with or without $CuCl_2$; **L1**, C with **L1**; **L2**, C with **L2**; **L3**, C + **L3**. The original gel images are shown in *SI Appendix*, Fig. S24*A*. Conditions were as follows: [Aβ], 25 μM; [$CuCl_2$], 25 μM; [compound], 50 μM; 37 °C, constant agitation. (*C*) Morphologies of Cu(II)-bound $Aβ_{40}$ aggregates from *B*, monitored by TEM. (Scale bars, 200 nm.)

Two types of experiments were conducted employing $Aβ_{40}$ and $Aβ_{42}$, two major isoforms of Aβ (18): 1) inhibition experiments (Fig. 4*A*): freshly prepared Aβ species were treated with **L1**, **L2**, and **L3** in the absence and presence of Cu(II) for 24 h; and 2) disaggregation experiments (*SI Appendix*, Fig. S20*A*): Aβ peptides were preincubated with or without Cu(II) for 24 h followed by introduction of the compounds for an additional 24 h.

In the inhibition experiments, the aggregation of both Cu(II)–$Aβ_{40}$ and Cu(II)–$Aβ_{42}$ was altered by **L1** under aerobic conditions, as illustrated in Fig. 4*B*. When **L1** was incubated with Cu(II)-treated Aβ species, noticeable smearing bands were indicated in the gel/Western blots, compared to those obtained with compound-free Cu(II)–Aβ samples. The resultant Aβ aggregates produced in the presence of **L1** were visualized by TEM to be shorter fibrils or amorphous aggregates, relative to compound-free Cu(II)–Aβ samples, as indicated in Fig. 4*C* and *SI Appendix*, Fig. S21*B*. Additionally, upon incubation of **L1** with Cu(II)–$Aβ_{40}$, the signal of an anti-oligomer antibody (A11), able to detect structured oligomers (54), was reduced, further supporting the alteration of Cu(II)-mediated Aβ aggregation by treatment of **L1** (*SI Appendix*, Fig. S21*C*). In the absence of O_2, **L1** did not affect the aggregation of Cu(II)–Aβ (Fig. 4 *B*, *Right*). Furthermore, the aggregation of metal-free $Aβ_{40}$ and $Aβ_{42}$ was not modulated by **L1** (Fig. 4*B* and *SI Appendix*, Fig. S22). Moreover, as expected from ESI–MS studies (vide supra), **L2** and **L3** were not able to vary the aggregation of both Cu(II)-added $Aβ_{40}$/$Aβ_{42}$ and metal-free $Aβ_{40}$/$Aβ_{42}$, which was confirmed by gel/Western blots and TEM (Fig. 4 and *SI Appendix*, Figs. S21 and S22).

The disassembly or modulation of further aggregation of preformed Cu(II)-treated and metal-free Aβ aggregates by the compounds was also investigated (*SI Appendix*, Figs. S20 and S23). Similar to the inhibition studies, in the disaggregation experiments, the gel/Western blots showed 1) the noticeable smearing bands in preformed Cu(II)-treated $Aβ_{40}$ and $Aβ_{42}$ aggregates in the presence of **L1** and 2) no influence of **L1** on preformed metal-free $Aβ_{40}$ and $Aβ_{42}$ aggregates. Short Aβ fibrils were monitored by TEM upon treatment of preformed Cu(II)–Aβ aggregates with **L1**, while long and large Aβ fibrils were still found under metal-free conditions. Moreover, **L2** and **L3** exhibited no effects on preformed Cu(II)–$Aβ_{40}$/$Aβ_{42}$ and metal-free $Aβ_{40}$/$Aβ_{42}$ aggregates according to the data obtained by gel/Western blots and TEM. Collectively, the aggregation of both Cu(II)–$Aβ_{40}$ and Cu(II)–$Aβ_{42}$ was noticeably impacted by **L1**, while **L2** and **L3** could not significantly affect Aβ aggregation even in the presence of Cu(II).

Regulation of the Toxicity Triggered by Cu(II)–Aβ, Free Organic Radicals, and ROS. To determine the effect of **L1** on the toxicity of Cu(II)–Aβ, the MTT assay employing a human neuroblastoma SH-SY5Y cell line was carried out [MTT: 3-(4,5-dimethylthiazol-2-yl)-2,5-diphenyltetrazolium bromide]. For the cytotoxicity studies, Aβ with either Cu(II), **L1**, or both was preincubated for 24 h, and the resultant samples were treated to SH-SY5Y cells. As shown in Fig. 5, cell toxicity of the $Aβ_{40}$ species generated with Cu(II) and **L1** was reduced by approximately 15 to 20%, relative to that of compound-free Cu(II)–$Aβ_{40}$. In the case of Cu(II)-treated $Aβ_{42}$, cell viability was slightly increased by **L1** under our experimental conditions (approximately 5%; *SI Appendix*, Fig. S25*A*). The cytotoxicity of metal-free $Aβ_{40}$ and $Aβ_{42}$ was lowered by less than 10% upon treatment of **L1**. In addition to **L1**, the effects of other copper chelators, i.e., 2,2′,2″,2‴-(ethane-1,2-diyldinitrilo)tetraacetic acid (**EDTA**) and 1,10-phenanthroline (**phen**), on the cytotoxicity of Cu(II)–$Aβ_{40}$ and metal-free $Aβ_{40}$ were also evaluated (Fig. 5 and *SI Appendix*, Fig. S25*B*). Cell survival of the $Aβ_{40}$ samples incubated with the two chelators in the absence and presence of Cu(II) was equal to or lower than that of compound-free samples under our experimental conditions. These overall results support that **L1**-mediated modifications toward Cu(II)–Aβ could reduce

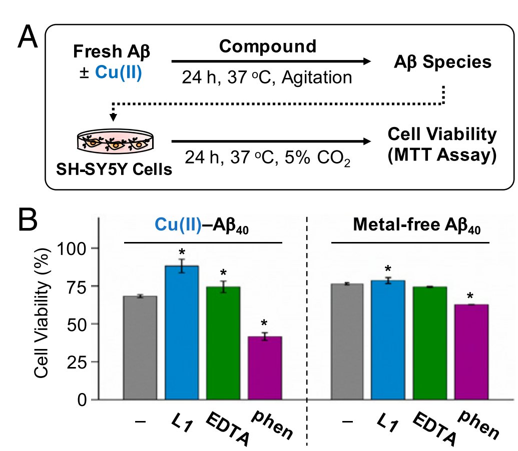

Fig. 5. Regulation of the toxicity triggered by Cu(II)-treated $Aβ_{40}$ and metal-free $Aβ_{40}$ by **L1** and other metal chelators (i.e., **EDTA** and **phen**) in living cells. (*A*) Scheme of the cell viability experiments. (*B*) Survival of the cells treated with Cu(II)-added $Aβ_{40}$ and metal-free $Aβ_{40}$ that were preincubated with **L1**, **EDTA**, and **phen**. Cell viability, determined by the MTT assay, was calculated in comparison to that with an equivalent amount of DMSO. Conditions were as folows: [$Aβ_{40}$], 10 μM, [$CuCl_2$], 10 μM, [compound], 10 μM. *$P < 0.05$ by Student's *t* test.

the cytotoxicity induced by the metal–Aβ complex. Note that **L1**, **L2**, and **L3** are relatively less toxic showing higher than 80% of cell survival up to 25 μM, as presented in *SI Appendix*, Fig. S26.

In addition to modifying Aβ, the antioxidant activity of **L1** may also contribute toward the molecule's cytoprotective effects based on its redox properties (32, 55). The regulation of free organic radicals by the compounds was monitored by the Trolox equivalent antioxidant capacity (TEAC) assay. The TEAC value indicates the ability of compounds to quench free organic radicals such as $ABTS^{+\bullet}$, relative to that of Trolox, a vitamin E analog [ABTS: 2,2′-azino-bis(3-ethylbenzothiazoline-6-sulfonic acid); Trolox: 6-hydroxy-2,5,7,8-tetramethylchroman-2-carboxylic acid] (56). The TEAC value of **L1** was 1.86 (± 0.10), while those of **L2** and **L3** were 0.86 (± 0.10) and 0.96 (± 0.13), respectively. The trend of the compounds' antioxidant properties is correlated to their E_{pa} values, indicated in Fig. 3*C*. These observations are consistent with the previous reports regarding a relation between the redox properties of compounds and their antioxidant capabilities (32, 55).

Moreover, the ability of **L1** to 1) remove ROS and 2) inhibit the production of ROS by Fenton-like reactions of Cu(I/II)–Aβ was evaluated. The quantity of H_2O_2, as a ROS, was measured by the absorption of resorufin, a red chromophore produced by the reaction of Amplex Red and H_2O_2 in a 1:1 stoichiometry in the presence of peroxidase (57). As shown in *SI Appendix*, Fig. S27*A*, **L1** was able to reduce the amount of H_2O_2 in a concentration-dependent manner. Furthermore, **L1** could scavenge H_2O_2 generated from Cu(I/II) with and without $Aβ_{40}$ in the presence of a reducing agent (e.g., *L*-ascorbate; *SI Appendix*, Fig. S27*B*). Note that the samples of Cu(II)–$Aβ_{40}$ with and without **L1** in the absence of *L*-ascorbate did not generate detectable amounts of H_2O_2 (*SI Appendix*, Fig. S27*B*). The notable decrease in the levels of H_2O_2 upon treatment of **L1** may be a consequence of 1) the antioxidant capability of **L1** itself based on its redox potential; 2) the antioxidant activity of **DMPD**, an *N*-dealkylation product of **L1** (31); or 3) the **L1**-directed regulation of Fenton-like reactions of Cu(I/II) or Cu(I/II)–Aβ (58). Overall, the TEAC and H_2O_2 assays demonstrate the ability of **L1** to scavenge free organic radicals and ROS, along with its potential to control Cu(I/II)- or Cu(I/II)–Aβ-mediated production of ROS.

Discussion

Cu(II)–Aβ complexes represent a pathological connection between Aβ and metal ions in AD (2, 4, 8–12, 15). Recent findings indicate that Cu(II)–Aβ could directly contribute toward neurodegeneration through the production of toxic oligomers and ROS (2, 4, 15, 19, 20). Based on the potential neurotoxic implications of Cu(II)–Aβ, research endeavors have led to the development of several chemical reagents [e.g., N^1-(pyridin-2-ylmethyl)benzene-1,4-diamine (**1**), N^1,N^1-dimethyl-N^4-(quinolin-2-ylmethyl)benzene-1,4-diamine (**3**), and N^1,N^1-dimethyl-N^4-(pyridin-2-ylmethyl) benzene-1,4-diamine (**L2-b**)] reported to alter the aggregation of Cu(II)–Aβ by triggering the modifications of Aβ (27, 29). The abovementioned molecules are able to form a ternary complex with Cu(II)–Aβ and elicit the oxidative degradation of Aβ (27, 29), and **1** and **3** were able to oxidize Aβ (29). The exact locations of such peptide modifications against Cu(II)–Aβ with respect to the transformed amino acid residue have not been fully identified, however. In this study, an effective mechanistic approach was developed to chemically modify the coordination sphere of Cu(II)–Aβ with a rationally designed molecule, **L1**, by binding to the metal–peptide complex and promoting copper–O_2 chemistry at the metal center. This study presents experimental evidence that the His14 residue in Cu(II)–Aβ was specifically modified via either covalent bond formation, oxidation, or both. It should be noted that the **L1**-induced dual-modification (both covalent bond formation and oxidation) at His14 was not observed against Aβ in the presence of 1) other metal ions [i.e., Fe(II), Fe(III), Co(II), and Zn(II)] and 2) other proteins (i.e., α-Syn and hIAPP [amyloidogenic] as well as ubiquitin [nonamyloidogenic]) even with treatment of Cu(II). Considering the neurotoxic implications of the interactions between Cu(I/II) and Aβ, such modifications at the coordination sphere of Cu(II)–Aβ could effectively alter the properties of the metal–Aβ complex. As expected, the aggregation and toxicity profiles of the resultant products from the reaction between Cu(II)–Aβ and **L1** under aerobic conditions were significantly modulated. Overall, our multidisciplinary studies with emphasis on approaches, reactivities, and mechanisms demonstrate a direction for modulating Cu(II)–Aβ complexes related to the pathology of AD.

Materials and Methods

All reagents were purchased from commercial suppliers and used as received unless otherwise noted. $Aβ_{40}$ and $Aβ_{42}$ ($Aβ_{42}$: DAEFRHDSGYEVHHQKLVFFAEDVGSNKGAIIGLMVGGVVIA) were purchased from Anaspec (Fremont, CA) or Peptide Institute, Inc. (Osaka, Japan). **EDTA** and **phen** were purchased from Sigma-Aldrich (St. Louis, MO) and Thermo Fisher Scientific (Waltham, MA), respectively. Trace metal ions were removed from the solutions used for the studies by treatment with Chelex overnight (Sigma-Aldrich). ESI–MS and ESI–MS^2 analyses were performed by an Agilent 2530 mass spectrometry dual AJS-ESI (Santa Clara, CA) or a Waters Synapt G2-Si quadrupole time-of-flight ion-mobility mass spectrometer (Waters, Manchester, UK) equipped with an ESI source (Daegu Gyeongbuk Institute of Science & Technology Center for Core Research Facilities, Daegu, Republic of Korea). CD spectra were obtained by a J-815 spectropolarimeter (Korea Advanced Institute of Science and Technology Analysis Center for Research Advancement [KARA], Daejeon, Republic of Korea). UV–vis spectra were recorded on an Agilent 8453 UV–vis spectrophotometer. Cyclic voltammograms were obtained under N_2 (g) on a CHI620E potentiostat (Qrins, Seoul, Republic of Korea). The concentration of copper in solution was measured by an Agilent ICP–MS 7700S (KARA). TEM images were taken by a JEOL JEM-2100 transmission electron microscope (Ulsan National Institute of Science and Technology Central Research Facilities [UCRF], Ulsan, Republic of Korea). Absorbance values for biological assays were obtained by a Molecular Devices SpectraMax M5e microplate reader (Sunnyvale, CA). ^1H and ^{13}C nuclear magnetic resonance (NMR) spectra were recorded on a 400-MHz Agilent NMR spectrometer (UCRF). The high-resolution mass spectra of compounds were taken by a Q Exactive Plus Orbitrap mass spectrometer (Thermo Fisher Scientific). The details of experimental procedures and methods are presented in *SI Appendix*. All data discussed in this study are included in the main text and *SI Appendix*.

ACKNOWLEDGMENTS. This work was supported by the National Research Foundation of Korea (NRF), funded by the Korean government (Grants NRF-2016R1A5A1009405 and NRF-2017R1A2B3002585 [to M.H.L.] and NRF-2015R1D1A1A01060188 [to J.C.]). J.H. acknowledges the Global Ph.D. Fellowship Program for support through the NRF, funded by the Ministry of Education (Grant NRF-2019H1A2A1073754).

1. E. L. Que, D. W. Domaille, C. J. Chang, Metals in neurobiology: Probing their chemistry and biology with molecular imaging. *Chem. Rev.* **108**, 1517–1549 (2008).
2. M. G. Savelieff *et al*., Development of multifunctional molecules as potential therapeutic candidates for Alzheimer's disease, Parkinson's disease, and amyotrophic lateral sclerosis in the last decade. *Chem. Rev.* **119**, 1221–1322 (2019).
3. C. J. Chang, Searching for harmony in transition-metal signaling. *Nat. Chem. Biol.* **11**, 744–747 (2015).
4. K. P. Kepp, R. Squitti, Copper imbalance in Alzheimer's disease: Convergence of the chemistry and the clinic. *Coord. Chem. Rev.* **397**, 168–187 (2019).
5. K. J. Barnham, C. L. Masters, A. I. Bush, Neurodegenerative diseases and oxidative stress. *Nat. Rev. Drug Discov.* **3**, 205–214 (2004).
6. I. F. Scheiber, J. F. B. Mercer, R. Dringen, Metabolism and functions of copper in brain. *Prog. Neurobiol.* **116**, 33–57 (2014).
7. E. Nam, J. Han, J.-M. Suh, Y. Yi, M. H. Lim, Link of impaired metal ion homeostasis to mitochondrial dysfunction in neurons. *Curr. Opin. Chem. Biol.* **43**, 8–14 (2018).
8. A. I. Bush, C. L. Masters, R. E. Tanzi, Copper, β-amyloid, and Alzheimer's disease: Tapping a sensitive connection. *Proc. Natl. Acad. Sci. U.S.A.* **100**, 11193–11194 (2003).
9. P. Faller, C. Hureau, G. La Penna, Metal ions and intrinsically disordered proteins and peptides: From Cu/Zn amyloid-β to general principles. *Acc. Chem. Res.* **47**, 2252–2259 (2014).
10. M. G. Savelieff, S. Lee, Y. Liu, M. H. Lim, Untangling amyloid-β, tau, and metals in Alzheimer's disease. *ACS Chem. Biol.* **8**, 856–865 (2013).
11. P. Faller, C. Hureau, O. Berthoumieu, Role of metal ions in the self-assembly of the Alzheimer's amyloid-β peptide. *Inorg. Chem.* **52**, 12193–12206 (2013).
12. K. P. Kepp, Alzheimer's disease: How metal ions define β-amyloid function. *Coord. Chem. Rev.* **351**, 127–159 (2017).

13. S. C. Drew, K. J. Barnham, The heterogeneous nature of Cu^{2+} interactions with Alzheimer's amyloid-β peptide. *Acc. Chem. Res.* **44**, 1146–1155 (2011).
14. J.-M. Suh, G. Kim, J. Kang, M. H. Lim, Strategies employing transition metal complexes to modulate amyloid-β aggregation. *Inorg. Chem.* **58**, 8–17 (2019).
15. E. Atrián-Blasco *et al*., Cu and Zn coordination to amyloid peptides: From fascinating chemistry to debated pathological relevance. *Coord. Chem. Rev.* **375**, 38–55 (2018).
16. A. S. DeToma, S. Salamekh, A. Ramamoorthy, M. H. Lim, Misfolded proteins in Alzheimer's disease and type II diabetes. *Chem. Soc. Rev.* **41**, 608–621 (2012).
17. E. Sitkiewicz, M. Kłoniecki, J. Poznański, W. Bal, M. Dadlez, Factors influencing compact-extended structure equilibrium in oligomers of a$\beta_{1\text{-}40}$ peptide–An ion mobility mass spectrometry study. *J. Mol. Biol.* **426**, 2871–2885 (2014).
18. S. J. C. Lee, E. Nam, H. J. Lee, M. G. Savelieff, M. H. Lim, Towards an understanding of amyloid-β oligomers: Characterization, toxicity mechanisms, and inhibitors. *Chem. Soc. Rev.* **46**, 310–323 (2017).
19. D. G. Smith, R. Cappai, K. J. Barnham, The redox chemistry of the Alzheimer's disease amyloid β peptide. *Biochim. Biophys. Acta* **1768**, 1976–1990 (2007).
20. A. Rauk, The chemistry of Alzheimer's disease. *Chem. Soc. Rev.* **38**, 2698–2715 (2009).
21. K. Rajasekhar, C. Madhu, T. Govindaraju, Natural tripeptide-based inhibitor of multifaceted amyloid β toxicity. *ACS Chem. Neurosci.* **7**, 1300–1310 (2016).
22. T. Chen *et al*., Effects of cyclen and cyclam on zinc(II)- and copper(II)-induced amyloid β-peptide aggregation and neurotoxicity. *Inorg. Chem.* **48**, 5801–5809 (2009).
23. W. H. Wu *et al*., Sequestration of copper from β-amyloid promotes selective lysis by cyclen-hybrid cleavage agents. *J. Biol. Chem.* **283**, 31657–31664 (2008).
24. A. Robert, Y. Liu, M. Nguyen, B. Meunier, Regulation of copper and iron homeostasis by metal chelators: A possible chemotherapy for Alzheimer's disease. *Acc. Chem. Res.* **48**, 1332–1339 (2015).
25. Y. Liu, M. Nguyen, A. Robert, B. Meunier, Metal ions in Alzheimer's disease: A key role or not? *Acc. Chem. Res.* **52**, 2026–2035 (2019).
26. C. Esmieu *et al*., Copper-targeting approaches in Alzheimer's disease: How to improve the fallouts obtained from in vitro studies. *Inorg. Chem.* **58**, 13509–13527 (2019).
27. M. W. Beck *et al*., A rationally designed small molecule for identifying an *in vivo* link between metal-amyloid-β complexes and the pathogenesis of Alzheimer's disease. *Chem. Sci.* **6**, 1879–1886 (2015).
28. S. Hong *et al*., Advanced electron paramagnetic resonance studies of a ternary complex of copper, amyloid-β, and a chemical regulator. *Inorg. Chem.* **57**, 12665–12670 (2018).
29. M. W. Beck *et al*., Structure-mechanism-based engineering of chemical regulators targeting distinct pathological factors in Alzheimer's disease. *Nat. Commun.* **7**, 13115 (2016).
30. D. J. Hayne, S. Lim, P. S. Donnelly, Metal complexes designed to bind to amyloid-β for the diagnosis and treatment of Alzheimer's disease. *Chem. Soc. Rev.* **43**, 6701–6715 (2014).
31. J. S. Derrick *et al*., A redox-active, compact molecule for cross-linking amyloidogenic peptides into nontoxic, off-pathway aggregates: In vitro and in vivo efficacy and molecular mechanisms. *J. Am. Chem. Soc.* **137**, 14785–14797 (2015).
32. J. Han *et al*., Tuning structures and properties for developing novel chemical tools toward distinct pathogenic elements in Alzheimer's disease. *ACS Chem. Neurosci.* **9**, 800–808 (2018).
33. D. Jiang *et al*., Redox reactions of copper complexes formed with different β-amyloid peptides and their neuropathalogical relevance. *Biochemistry* **46**, 9270–9282 (2007).
34. M. Y. Combariza, R. W. Vachet, Gas-phase ion-molecule reactions of transition metal complexes: The effect of different coordination spheres on complex reactivity. *J. Am. Soc. Mass Spectrom.* **13**, 813–825 (2002).
35. C. E. Elwell *et al*., Copper–oxygen complexes revisited: Structures, spectroscopy, and reactivity. *Chem. Rev.* **117**, 2059–2107 (2017).
36. J. Y. Lee, K. D. Karlin, Elaboration of copper-oxygen mediated C-H activation chemistry in consideration of future fuel and feedstock generation. *Curr. Opin. Chem. Biol.* **25**, 184–193 (2015).
37. S. Itho, "Chemical reactivity of copper active-oxygen complexes" in *Copper-Oxygen Chemistry*, K. D. Karlin, S. Itho, S. Rokita, Eds. (Wiley on Reactive Intermediates in Chemistry and Biology, John Wiley & Sons, 2011) pp. 225–282.
38. S. Kim *et al*., Amine oxidative *N*-dealkylation via cupric hydroperoxide Cu-OOH homolytic cleavage followed by site-specific fenton chemistry. *J. Am. Chem. Soc.* **137**, 2867–2874 (2015).
39. M. Sato *et al*., Site-specific inhibitory mechanism for amyloid β_{42} aggregation by catechol-type flavonoids targeting the Lys residues. *J. Biol. Chem.* **288**, 23212–23224 (2013).
40. L. Di, E. H. Kerns, K. Fan, O. J. McConnell, G. T. Carter, High throughput artificial membrane permeability assay for blood-brain barrier. *Eur. J. Med. Chem.* **38**, 223–232 (2003).
41. A. Avdeef *et al*., PAMPA–critical factors for better predictions of absorption. *J. Pharm. Sci.* **96**, 2893–2909 (2007).
42. D. L. Swaney, G. C. McAlister, J. J. Coon, Decision tree-driven tandem mass spectrometry for shotgun proteomics. *Nat. Methods* **5**, 959–964 (2008).
43. S.-M. Liao, Q.-S. Du, J.-Z. Meng, Z.-W. Pang, R.-B. Huang, The multiple roles of histidine in protein interactions. *Chem. Cent. J.* **7**, 44 (2013).
44. D. P. Demarque, A. E. M. Crotti, R. Vessecchi, J. L. C. Lopes, N. P. Lopes, Fragmentation reactions using electrospray ionization mass spectrometry: An important tool for the structural elucidation and characterization of synthetic and natural products. *Nat. Prod. Rep.* **33**, 432–455 (2016).
45. F. Arrigoni *et al*., Copper reduction and dioxygen activation in Cu-amyloid beta peptide complexes: Insight from molecular modelling. *Metallomics* **10**, 1618–1630 (2018).
46. N. Hewitt, A. Rauk, Mechanism of hydrogen peroxide production by copper-bound amyloid beta peptide: A theoretical study. *J. Phys. Chem. B* **113**, 1202–1209 (2009).
47. C. Schöneich, Mechanisms of metal-catalyzed oxidation of histidine to 2-oxo-histidine in peptides and proteins. *J. Pharm. Biomed. Anal.* **21**, 1093–1097 (2000).
48. M. J. Davies, Protein oxidation and peroxidation. *Biochem. J.* **473**, 805–825 (2016).
49. M. Palmblad, A. Westlind-Danielsson, J. Bergquist, Oxidation of methionine 35 attenuates formation of amyloid β -peptide 1-40 oligomers. *J. Biol. Chem.* **277**, 19506–19510 (2002).
50. J. Kang *et al*., Chemical strategies to modify amyloidogenic peptides using iridium(iii) complexes: Coordination and photo-induced oxidation. *Chem. Sci.* **10**, 6855–6862 (2019).
51. R. Kayed *et al*., Fibril specific, conformation dependent antibodies recognize a generic epitope common to amyloid fibrils and fibrillar oligomers that is absent in prefibrillar oligomers. *Mol. Neurodegener.* **2**, 18 (2007).
52. J.-S. Choi, J. J. Braymer, R. P. Nanga, A. Ramamoorthy, M. H. Lim, Design of small molecules that target metal-Aβ species and regulate metal-induced Aβ aggregation and neurotoxicity. *Proc. Natl. Acad. Sci. U.S.A.* **107**, 21990–21995 (2010).
53. J. S. Derrick *et al*., Mechanistic insights into tunable metal-mediated hydrolysis of amyloid-β peptides. *J. Am. Chem. Soc.* **139**, 2234–2244 (2017).
54. R. Kayed *et al*., Common structure of soluble amyloid oligomers implies common mechanism of pathogenesis. *Science* **300**, 486–489 (2003).
55. S. Chevion, M. A. Roberts, M. Chevion, The use of cyclic voltammetry for the evaluation of antioxidant capacity. *Free Radic. Biol. Med.* **28**, 860–870 (2000).
56. H. J. Lee *et al*., Structural and mechanistic insights into development of chemical tools to control individual and inter-related pathological features in Alzheimer's disease. *Chemistry* **23**, 2706–2715 (2017).
57. M. Zhou, Z. Diwu, N. Panchuk-Voloshina, R. P. Haugland, A stable nonfluorescent derivative of resorufin for the fluorometric determination of trace hydrogen peroxide: Applications in detecting the activity of phagocyte NADPH oxidase and other oxidases. *Anal. Biochem.* **253**, 162–168 (1997).
58. E. Atrián-Blasco, M. Del Barrio, P. Faller, C. Hureau, Ascorbate oxidation by Cu(amyloid-β) complexes: Determination of the intrinsic rate as a function of alterations in the peptide sequence revealing key residues for reactive oxygen species production. *Anal. Chem.* **90**, 5909–5915 (2018).